American Mineralogist, Volume 91, pages 1565–1573, 2006

Pyroxene europium valence oxybarometer: Effects of pyroxene composition, melt composition, and crystallization kinetics

C.K. SHEARER,* J.J. PAPIKE, AND J.M. KARNER

Institute of Meteoritics, Department of Earth and Planetary Sciences, University of New Mexico, Albuquerque, New Mexico 87131-1126, U.S.A.

ABSTRACT

The behavior of multivalent elements such as Fe, Cr, V, and Eu in magmatic systems reflects the f_{O_2} of the environment. In particular, Eu behavior in pyroxene from basaltic systems has been demonstrated to be an effective measure of f_{O_2}. We selected two nearly isochemical lunar pigeonite basalts (15058, 15499), a lunar high-Ti basalt (75035), and Pasamonte (representing asteroid 4 Vesta, an unequilibrated eucrite), to explore other potential variables that may affect this indicator of f_{O_2}. All of these basalts crystallized at an f_{O_2} of approximately IW-1, yet they experienced different cooling and crystallization histories and their pyroxenes exhibit a wide range of compositional trajectories within the pyroxene quadrilateral. There are several variables that influence the Eu/Eu* recorded in pyroxene that may compromise the determination of f_{O_2}. Previous experimental studies show that pyroxene composition influences the ability of pyroxene to accommodate REE and fractionate Eu^{2+} from Eu^{3+}. We demonstrate that in addition to the influence of Ca in the M2 site, the Al content in the pyroxene and its influence on coupled substitutions will also influence the fractionation of Eu^{2+} from Eu^{3+}. For example, the coupled substitution $^{T}Si^{4+} + {}^{M2}R^{2+} \rightarrow {}^{T}Al^{3+} + {}^{M2}REE^{3+}$ may accommodate REE^{3+} in preference to Eu^{2+}, which is too large. Different pyroxene growth surfaces will incorporate Eu^{2+} and Eu^{3+} differently due to differences in growth rate, Al content, and site configuration. In consort with the pyroxene composition, fractionation of Eu^{2+} from Eu^{3+} will be aided by the Al content of the basaltic melt, which increases the activities of network-forming components such as $CaAl_2O_4$ and $FeAl_2O_4$ in the melt during pyroxene crystallization. The Al content will result in changing the partitioning behavior of Eu^{3+} while having very little effect on Eu^{2+}. Melt composition, the appearance of plagioclase on the liquidus, and the kinetics of plagioclase crystallization are influenced by cooling rate. Data from the four basalts selected also suggest that Eu^{2+}/Eu^{3+} in the melt remains buffered even with extreme differences in cooling rate and plagioclase crystallization kinetics. Unexpectedly, many of these same variables affect the substitution of multivalent V. If the f_{O_2} determined from Eu behavior in pyroxene is not placed within a petrologic and crystal-chemical context, errors of 1 to 2 log units may result. The influence of these variables may be reduced by using multiple, co-crystallizing phases (i.e., plagioclase and pyroxene) and ratioing D_{Eu} to adjacent REE ($D_{Sm, Gd}$).

Keywords: Eu valence, V valence, pyroxene, oxybarometer, Moon, 4 Vesta

INTRODUCTION

The behavior of multivalent elements such as Fe, Cr, V, and Eu in magmatic systems reflects the f_{O_2} of the environment (Fig. 1; cf. Papike et al. 2005). The oxidation state of these elements will influence the mineral assemblage (i.e., magnetite vs. Fe-metal) (Papike et al. 1998), crystallization sequence (i.e., early vs. late spinel) (McKay et al. 2004), and element partitioning (i.e., partitioning of Cr and V in olivine and spinel) (Shearer et al. 2005). The effect of f_{O_2} on the relative proportions of divalent and trivalent Eu has proven to be a useful tool for estimating f_{O_2} in a variety of magmatic systems (Fig. 1). This dependence of the ratio Eu^{2+}/Eu^{3+} on f_{O_2} can be illustrated by the reaction: $Eu^{3+} + 1/2O^{2-} \rightarrow Eu^{2+} + 1/4O_2$. The concept of using Eu valence as a quantitative oxybarometer was initially demonstrated by Philpotts (1970) and Schnetzler and Philpotts (1970). The variation of $D_{Eu}^{plagioclase\text{-}melt}$ with oxygen fugacity has been determined experimentally by several workers and used to infer the redox conditions under which magmas have crystallized (e.g., Weill and Drake 1973; Weill et al. 1974; Drake 1975; Weill and McKay 1975). McKay (1989) experimentally calibrated the $D_{Eu}^{plagioclase\text{-}melt}$ and $D_{Eu}^{pyroxene\text{-}melt}$ for angrite melt compositions. That study not only demonstrated the power of using both minerals for estimating the redox conditions of angrite crystallization, but also hinted at the effect of melt composition on the behavior of Eu. Detailed crystal-chemical rationales for REE and Eu behavior in pyroxenes from lunar basalts were explored by Shearer and Papike (1989). The behavior of Eu in Martian basalts has been demonstrated to be an effective measure of f_{O_2} (Wadhwa 2001). $D_{Eu}^{pyroxene\text{-}melt}$ has been calibrated experimentally for Martian basalts by McKay et al. (1986), McCanta and Rutherford (2002), and Musselwhite et al. (2003, 2004). These studies have demonstrated both the power of Eu valence as an oxybarometer and its dependence on several magmatic and mineralogical variables.

Here, we evaluate the effect of pyroxene and melt composition, crystallization sequence, and crystallization kinetics

* E-mail: cshearer@unm.edu

0003-004X/06/0010–1565$05.00/DOI: 10.2138/am.2006.2098

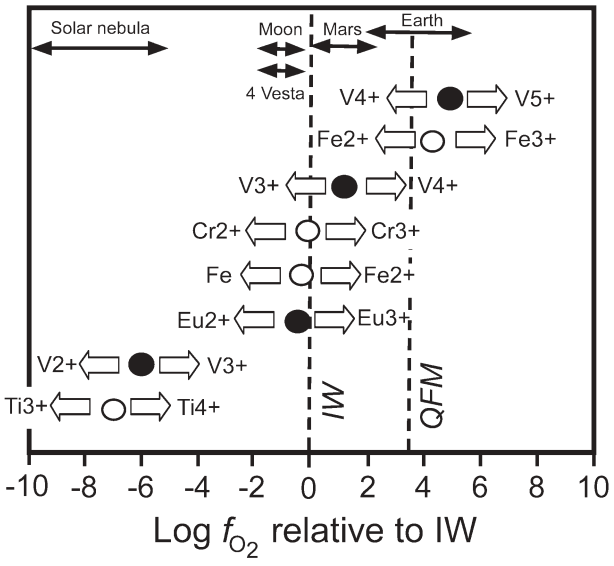

FIGURE 1. The diagram, adapted from Papike et al. (2005), illustrates some of the most important multivalent cations in basaltic systems and the range of f_{O_2} over which they are dominant. The individual points represent f_{O_2} conditions where the proportion of the two cations is approximately 50%. Filled points represent multivalent cation pairs (Eu and V) that are discussed in the text.

on the behavior Eu in natural basalts from similar, reducing environments (one log unit below the iron-wüstite = IW-1) of the Moon and the HED parent body (presumably 4 Vesta) and assess the influence of these variables on Eu valence as an oxybarometer. In addition, we compare the relationship between the behavior of Eu and the behavior of V, another multivalent element (V^{5+},V^{4+}, V^{3+}, and V^{2+}) in pyroxene (see also Karner et al. 2006a, this volume).

EXPERIMENTAL DESIGN AND ANALYTICAL APPROACH

To compare Eu^{2+}/Eu^{3+} in lunar basalts and eucrites and to understand better the variables that may affect this indicator of f_{O_2} in basalts, we selected two isochemical lunar pigeonite basalts (15058, 15499), a high-Ti lunar basalt (75035), and Pasamonte, an unequilibrated eucrite. All of these basalts crystallized at an f_{O_2} of approximately IW-1. Yet, they all have different cooling histories, crystallization histories, and pyroxene compositional trajectories within the pyroxene quadrilateral. The two lunar pigeonite basalts have experienced different cooling and crystallization histories (Bence and Papike 1972; Shearer et al. 1989). Basalt 15499 cooled at a rate of 5 to 20 °C/h, whereas 15058 cooled at a rate of <1 °C/h (Bence and Papike 1972). The high-Ti lunar basalt and the basalt clasts in Pasamonte represent basalts that had intermediate cooling rates (Papike et al. 1976; BVSP 1981).

All pyroxenes were imaged using back-scattered electrons (BSE) and mapped compositionally using scanning electron microscopy (SEM) and electron-microprobe (EMP) methods. A JEOL 5800LV SEM and a JEOL 8200 electron microprobe at the University of New Mexico were used to perform these analysis. Major elements were analyzed along core to rim traverses and across different growth surfaces. Imaging and major-element analyses were used to select strategically a smaller subset of points for trace-element ion-microprobe analyses. A Cameca 4f ims at the Institute of Meteoritics (IOM), University of New Mexico, was used to analyze Sm and Eu at all selected points. REE patterns (La, Ce, Nd, Sm, Eu, Dy, Er, and Yb) were determined in a smaller subset of points. Trace-element analyses were carried out using an O^- primary ion beam accelerated to 12.5 KeV. The beam current was set at 25 nA and resulted in a beam diameter of approximately 20 to 25 µm. The secondary ions were analyzed using moderate energy filtering (75 volts) and an energy window of ±25 V. Counting times on isotopes of interest were background = 2 s, ^{30}Si = 4 s, ^{147}Sm = 20 s, ^{151}Eu = 20 s, ^{153}Eu = 20 s, and other REE = 20 s. Each analysis consisted of 10 counting cycles. All concentrations were calculated from the empirical relationship between intensity ratios (i.e., $^{153}Eu/^{30}Si \times$ wt% SiO_2) and concentrations obtained from well-documented pyroxene standards (KAUG, KH1, C1-cpx) in the IOM lab. The calibration curve for Sm and Eu had a correlation coefficient of approximately 0.99. Accuracy and precision for the REE in the unknowns are 15% or better (generally better for the high-Ca pyroxene).

CHARACTERISTICS OF SELECTED BASALTS FROM THE MOON AND 4 VESTA

Numerous lines of evidence suggest that most lunar and eucritic basalts crystallized at f_{O_2} conditions of approximately IW-1. The presence of Fe metal or Ni,Fe alloys in these basalts indicates that they crystallized at f_{O_2} conditions below the iron-wüstite buffer. Absence of Fe^{3+} in both silicates and oxides and the occurrence of reduced valence states of Cr and Ti are consistent with the above observations (Papike et al. 1998, 2005). The quantitative measurement of reduced Cr, V, and Ti in lunar volcanic glasses (Shearer et al. 2004; Sutton et al. 2005; Karner et al. 2006b) and olivine in lunar basalts (Shearer et al. 2005) indicate these basalts crystallized at f_{O_2} conditions from IW-0.9 to IW-1.5. The metal-melt equilibria and the Cr content of the olivine (+spinel) were interpreted as indicating a pre-eruptive f_{O_2} of IW-1.3 for the lunar picritic glasses (Fogel et al. 1995). Intrinsic f_{O_2} measurements and thermodynamic gas-equilibria calculations demonstrate that the ranges of temperature and f_{O_2} for mare basalt crystallization are relatively small, varying from 10^{-13} at 1200 to 10^{-16} at 1000 °C (Sato 1976). Relative to standard buffer curves, these values are approximately 0.2 to 1.0 log units below iron-wüstite (IW) and above the univariant curve that defines the stability of ilmenite. The FeO content of the lunar basalts has been interpreted as indicating that the mare basalts were generated at an f_{O_2} of IW-1 (Jones 2004). The Cr content of liquids coexisting with spinel varies considerably with f_{O_2}, such that Cr is low (≈1000 ppm) at FMQ and high (>2700 ppm) at IW (Delano 1990). This variability is due to Cr^{2+} being less soluble in spinel in the mantle at reducing conditions and therefore remaining in the melt. The Cr content of primitive lunar basalts (2700–6300 ppm) is significantly higher than similar terrestrial basalts (<1500 ppm). Therefore, if spinel was a residual phase in the lunar mantle and the Cr content was near chondritic, the high Cr content of the mare basalts suggests a reduced lunar mantle (Papike and Bence 1978; Delano 1990; Hanson and Jones 1998).

The four basalts selected for this study exhibit different cooling rates, crystallization histories, and pyroxene compositional trajectories in the pyroxene quadrilateral. Two Apollo 15 pigeonite basalts (15058, 15499) contain complex clinopyroxene phenocrysts with pigeonite cores and augite rims immersed in a groundmass that ranges in texture from variolitic (15499) to subophitic (15058) (Figs. 2a and 2b). The average phenocryst grain size increases from 1–2 mm in (15499) to 1 cm in (15058). In the variolitic textured basalt, the phenocrysts have "hollow cores" and pigeonite "channelways" parallel to **c** (Bence et al. 1971). The textural differences between these two basalts have been attributed to differences in cooling history (Bence et al. 1971; Bence and Papike 1972; Lofgren et al. 1975). Lofgren et al. (1975) concluded that basalts with textures similar to 15499 cooled at a rate of 5 to 20 °C/h, whereas basalts with textures

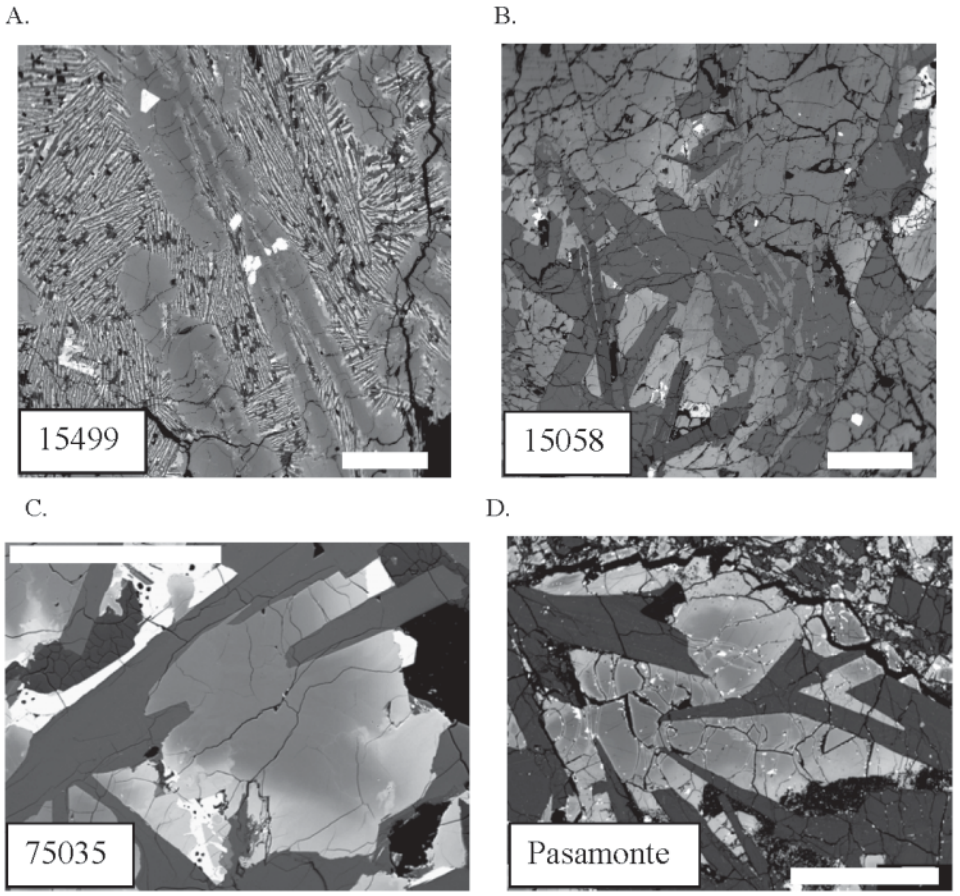

FIGURE 2. Back-scattered electron images of the four basalts used in this study. (**a**) Pigeonite basalt 15499 illustrating the vary late-stage crystallization of dark-gray plagioclase in variolitic intergrowth with bright oxide phases surrounding complexly zoned pyroxene. (**b**) Pigeonite basalt 15058 illustrating pyroxenes with substantial Fe-enrichment. Dark-gray plagioclase commonly grows from the pyroxene-melt interface. (**c**) High-Ti basalt 75035 illustrating anhedral pyroxene growing outward from a dark-gray plagioclase surface. Pyroxene exhibits extreme Fe-enrichment in bright rims. (**d**) Intergrown pyroxene and plagioclase in Pasamonte. Scale bar in all images is equal to 500 μm.

similar to 15058 cooled at a rate of less than 1 °C/h. The crystallization sequence of these two pigeonite basalts is pigeonite → augite → augite + plagioclase → ilmenite (Fig. 3). Crystallization of plagioclase in these two basalts is also influenced by cooling rate. In 15058, plagioclase penetrates into the outer augitic zones of the phenocrysts, whereas in 15499, plagioclase either occurs as elongate anhedral laths in the mesostasis or is not present at all.

An Apollo 17 high-Ti basalt is represented by sample 75035. This high-Ti basalt is medium-grained with a subophitic texture (Fig. 2c). The subhedral clinopyroxenes are approximately 0.4 to 0.6 mm in size and occur in an interlocking network of plagioclase and ilmenite. The clinopyroxene does not exhibit the complex zoning observed in the pigeonite basalts. Instead, the zoning is either concentric or extends from the pyroxene interface with earlier minerals (ilmenite or plagioclase) into the late-stage mesostasis. The crystallization sequence of this high-Ti-basalt is ilmenite → plagioclase → augite + plagioclase (Fig. 3). Metastable pyroxferroite crystallizes after the most Fe-rich pyroxene.

Pasamonte is an unequilibrated eucrite that potentially repre-

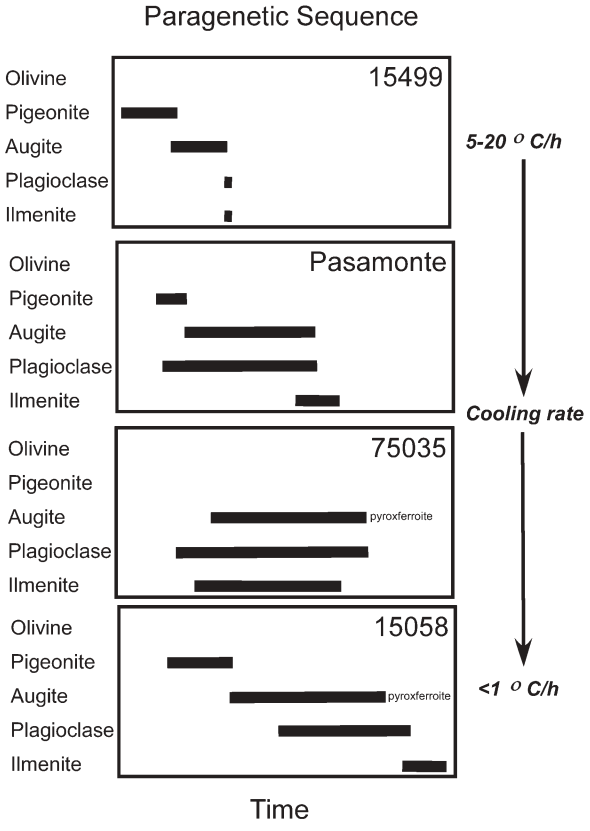

FIGURE 3. Paragenetic crystallization sequences for 15499, 15058, 75035, and Pasamonte. Note that plagioclase precedes pyroxene in two of the samples, but follows it in the other two.

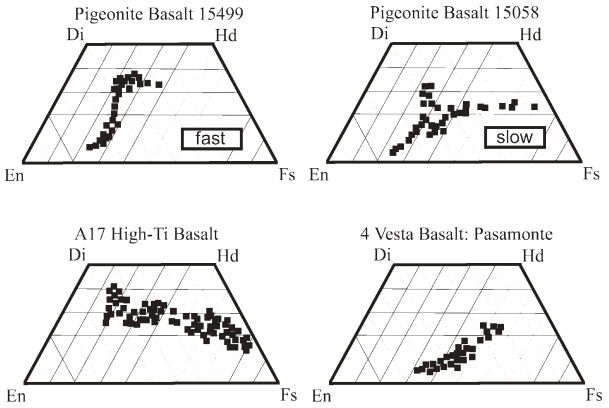

FIGURE 4. Pyroxene quadrilaterals illustrating pyroxene compositional trajectories for 15499, 15058, 75035, and Pasamonte.

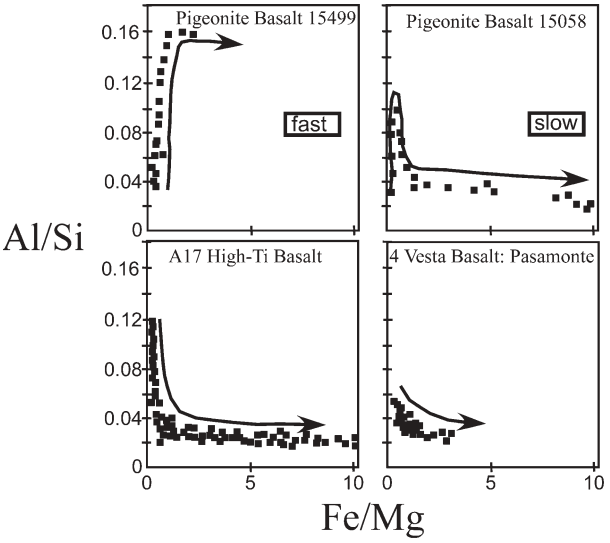

FIGURE 5. Al/Si vs. Fe/Mg cation ratios for pyroxene in the 4 basalts used in this study.

sents basaltic magmatism on asteroid 4 Vesta. Pasamonte has an FeO content similar to the above lunar basalts, but it is also higher in Al and lower in Ti, Ca/Al, and X_{Mg} [= Mg/(Mg + Fe)$_{atomic}$]. Pasamonte exhibits a subophitic texture in which the plagioclase occurs as laths that penetrate into or are partially surrounded by clinopyroxene (Fig. 2d). The subhedral to anhedral clinopyroxenes are approximately 0.3 to 0.6 mm in size. Pyroxene exhibits rather simple zoning with pigeonite cores zoned outward toward either pigeonite or augite rims. The crystallization sequence of Pasamonte is most likely pigeonite (?) → pigeonite + plagioclase → augite + plagioclase (Fig. 3). The cooling rates for the high-Ti lunar basalt and Pasamonte were intermediate to the two lunar pigeonite basalts, with the cooling rate of Pasamonte perhaps being somewhat greater than 75035.

ANALYTICAL RESULTS

Major elements

Major- and minor-element zoning characteristics (Figs. 4 and 5) of the pyroxenes in 15058, 15499, 75035, and Pasamonte have been described to varying degrees in the literature (e.g., Bence et al. 1970, 1971; Boyd and Smith 1971; Brett et al. 1971; Bence and Papike 1972; Papike et al. 1976; BVSP 1981; Shearer et al. 1989). Pyroxenes from the Apollo 15 pigeonite basalts have two compositional trends observed on the pyroxene quadrilateral: a Ca-enrichment trend with a variable discontinuity between pigeonite and augite normal to (110) of the pyroxene and a Ca-poor trend normal to (010) (Bence and Papike 1971, 1972). The Wo content of the pyroxene is related to the appearance of plagioclase in the crystallization sequence. Compared to the pyroxene in 15058, pyroxene in 15499 exhibits a slightly higher enrichment in Ca (Fig. 4). Also, pyroxene in 15058 exhibits a much more striking Fe-enrichment and depletion in Ca once plagioclase is a liquidus phase. In 15058, approximately 50% of the pyroxene phenocrysts crystallized prior to plagioclase, whereas in 15499, greater than 95% of the phenocrysts crystallized prior to plagioclase. Compositional zoning in 75035 and Pasamonte are far less complex (Fig. 4). Pyroxene in 75035 exhibits extreme Fe-enrichment associated with Ca depletion from core to rim. In contrast, pyroxene from Pasamonte exhibits moderate Fe-enrichment with an increase in Ca from pigeonite cores to augite rims (Fig. 4).

Plagioclase crystallization affects minor element zoning in pyroxene. In the two pigeonite basalts, early pigeonite has low Al/Si and Al/Ti (Bence and Papike 1972). With continued crystallization, these two ratios increase until plagioclase becomes a liquidus phase (Fig. 5). The increase in Al/Si generally reflects enrichment of the melt in Al prior to plagioclase saturation. Due to the difference in cooling rate, plagioclase crystallization in 15499 is delayed and results in extreme Al enrichments in the melt and pyroxene. Earlier plagioclase saturation in 15058 results in a dramatic decrease in Al/Si followed by a limited variation in this ratio with further Fe-enrichment. In basalt 75035, the Al/Si ratio exhibits only an initial decrease followed by a limited variation in this ratio with further Fe-enrichment. In Pasamonte, the earliest pigeonite has a somewhat varied Al content (1.4 to 2.2 wt% Al_2O_3) and the highest Al/Si and Al/Ti. The Al/Si decreases from core to rim (Fig. 5).

Trace elements

The REE behavior in pyroxenes from these basalts has been documented elsewhere by Shearer et al. (1989) and Pun and Papike (1995). In general, the low-Ca pyroxenes have LREE-depleted REE patterns. With increasing Ca in all of these pyroxenes, the LREE depletion is reduced and the overall REE abundance increases. This trend has been attributed to the effect of Ca substitution into the M2 site (Shearer et al. 1989), an effect that has been documented experimentally by McKay et al. (1986). With the Fe-enrichment exhibited by pyroxene in several of the basalts, the REE pattern remains the same, yet the abundance increases.

In this manuscript, our focus is on the behavior of divalent and trivalent Eu relative to the other trivalent REE. From the abundances of Sm and Eu, and the REE patterns, we calculated Eu/Eu* where Eu is the measured chondrite-normalized abundance and Eu* is the Eu abundance we would expect if all the Eu

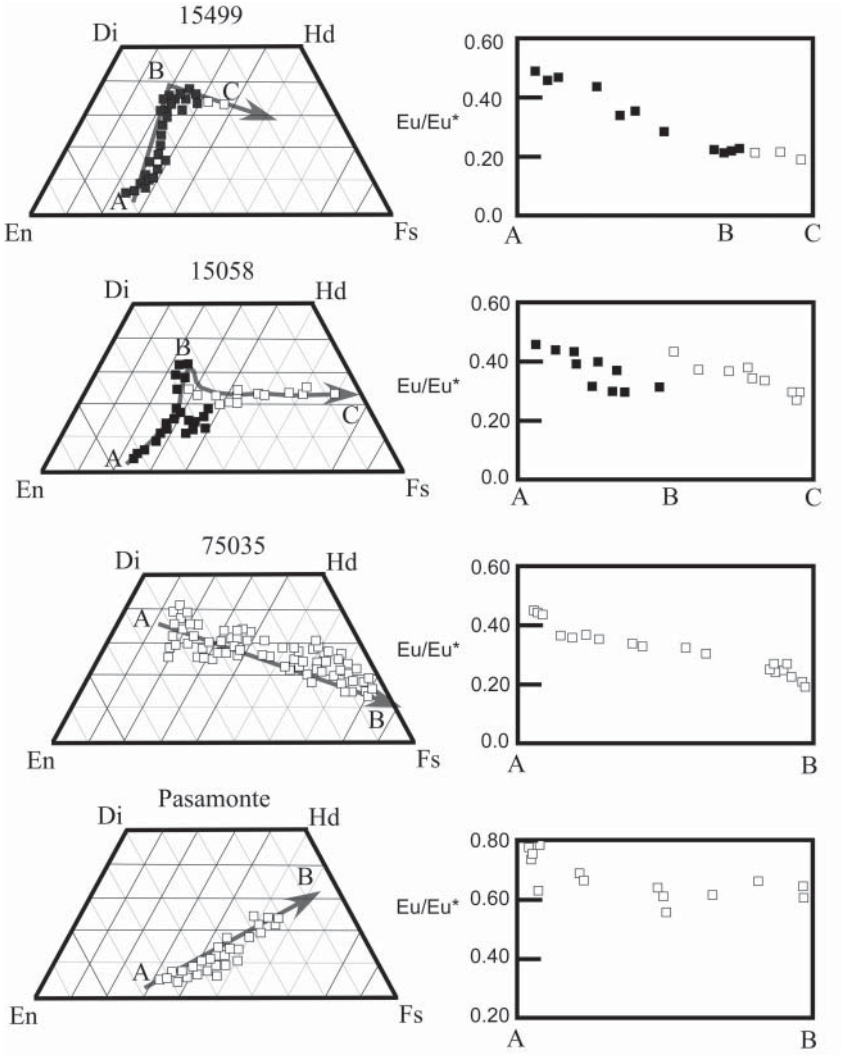

FIGURE 6. Relationships among pyroxene compositions in the quadrilateral, appearance of plagioclase as a liquidus phase, and Eu/Eu* for the four basalts used in this study. Open symbols represent pyroxenes that co-crystallized with plagioclase.

were trivalent. Eu/Eu* is 1 if there is no Eu anomaly, less than 1 if there is a negative Eu anomaly, and greater than 1 if the Eu anomaly is positive. All of the Eu/Eu* values in the pyroxenes analyzed in this study are less than 1. The smaller the value of Eu/Eu*, the more pronounced is the negative anomaly.

The relationship among Eu/Eu*, pyroxene composition, and onset of plagioclase crystallization is illustrated in Figure 6. The behavior of Eu/Eu* in pyroxenes from 15058 is much more complex than in the other basalts of this study. The Eu/Eu* decreases from approximately 0.44 to 0.30 with increasing Wo content in the pyroxene prior to the onset of plagioclase crystallization. Once plagioclase becomes a liquidus phase, Eu/Eu* increases abruptly and then decreases to the Fe-rich pyroxene rim. With increasing Ca content of the pyroxene, Eu/Eu* decreases more abruptly in the more quickly cooled pigeonite basalt (15499) compared to 15058 (0.46 to 0.22). The Eu/Eu* then remains constant in the rim of the pyroxene. The Eu/Eu* also appears to be different within different growth surfaces. For example, Eu/Eu* is greater in the sector normal to (110) than the sector normal to (010). In the high-Ti basalt represented by 75035, as the total REE abundances increase from the pyroxene Mg-rich cores toward the Fe-rich rims, the Eu/Eu* decreases from approximately 0.42 to 0.20. In Pasamonte, pyroxene cores appear to have variable Eu/Eu* that appears to correlate with Al abundance. The Eu/Eu* decreases slightly and then remains fairly constants with increasing Ca and Fe.

FACTORS CONTROLLING THE EU VALENCE RECORDED IN PYROXENE

Crystal chemistry of Eu in pyroxene

Pyroxene crystallizes in a variety of space groups, but for the purpose of this discussion, only three are important: *C*2/*c* for augite, $P2_1/c$ for pigeonite, and *Pbca* for orthopyroxene. The structures of all pyroxenes can be described in terms of alternating tetrahedral and octahedral layers parallel to the (100) plane. The tetrahedral layer is composed of infinite chains of corner-sharing tetrahedra running parallel to **c**. The "octahedral layer" is composed of the 6- to 8-coordinated M2 site and octahedral M1 site. The M1 octahedra share edges to form infinite chains parallel to **c**. The M2 polyhedra are either 6- or 8-coordinated depending on their occupancy. The site is 8-coordinated when it

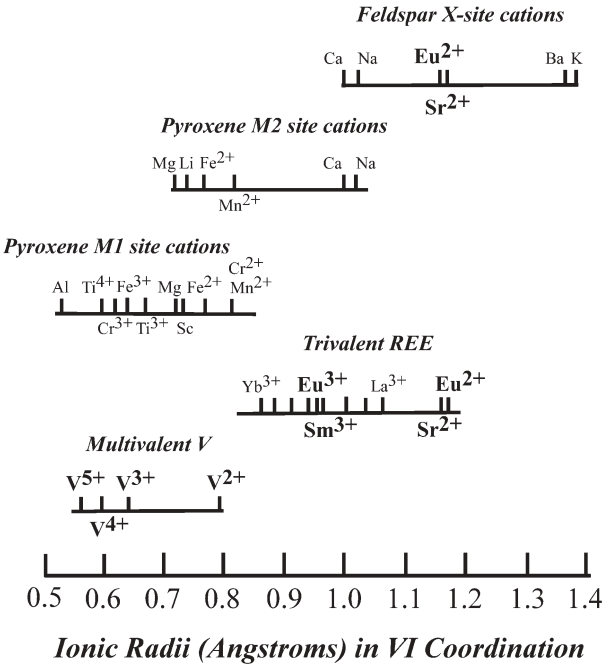

FIGURE 7. Comparison of ionic radii for Eu^{2+}, Eu^{3+}, and Sm with cations that occupy the M1 and M2 sites of pyroxene and the X site of plagioclase.

contains Ca or Na, but it is approximately 6-coordinated when containing Mn^{2+}, Fe^{2+}, Mg^{2+}, and Li^{+} cations (Fig. 7).

The three structural types considered here differ mainly in the manner in which the octahedral and tetrahedral layers are linked. These different topologies have a profound effect on the nature of the coordination and the size of the M2 site. The M2 site in augite and pigeonite has a great deal of flexibility to accommodate ions as large as Ca or Na in 8-coordination or as small as Mg in 6-coordination. This is in contrast to orthopyroxene (*Pbca*) in which the M2 site is not very flexible as a direct result of the octahedral stacking sequence (Cameron and Papike 1981).

Figure 7 illustrates the range of cation sizes that can be accommodated into the M1 and M2 site of pyroxene and the X site of feldspars. Based on these systematics, we would predict that Eu^{3+} should behave like many of the adjacent trivalent REE. It should be restricted to the pyroxene M2 site and be increasingly accommodated in that site with increasing Wo content of the pyroxene (Shearer et al. 1989). Divalent Eu must be totally excluded from the M2 site of orthopyroxene and is almost too large to fit in the expanded M2 site of augite. Obviously, it is well accommodated into the plagioclase X site. The extent of the substitution of Eu^{3+} and Eu^{2+} into the pyroxene structure was calculated by Shearer et al. (1989) using the assumptions of Philpotts (1970). They calculated that the Eu^{2+}/Eu^{3+} was approximately 0.03 in lunar pigeonite with approximately 10% Wo component.

Therefore, although basalts at f_{O_2} conditions of IW or at more reducing conditions have either Eu^{2+} and Eu^{3+} in subequal proportions or are enriched in Eu^{2+} (Fig. 1), it appears that the contrasting site characteristics in pyroxene and plagioclase result in an efficient separation of Eu^{2+} and Eu^{3+}. Clearly, pyroxene composition and the appearance of plagioclase on the liquidus play an important role in determining Eu/Eu* in pyroxene. Are these the only important factors? What is the response of the Eu^{2+}/Eu^{3+} in the melt during crystallization of phases that fractionate Eu^{2+} and Eu^{3+} to different degrees?

Pyroxene and melt compositions

Based on the above observations of the pyroxene structure, the M2 site of pyroxene should be able to increasingly accommodate both Eu^{2+} and Eu^{3+} with increasing Ca in the M2 site. The relative accommodation of these two cations into the M2 site as Ca content increases can be examined initially using an analogy to the behavior of Sr^{2+} ($\approx Eu^{2+}$) and Sm^{3+} ($\approx Eu^{3+}$). Experimental determination of D_{Sm} in pyroxene indicates that it increases an order of magnitude (i.e., 0.02 to 0.25) from Wo_{10} to Wo_{40} (McKay et al. 1986). Experimental determination of D_{Sr} over a similar range of pyroxene compositions indicates that it also increases by at least an order of magnitude (Weill and McKay 1975; Sobolev et al. 1996). This initial analysis implies that increasing the Wo content of the pyroxene does not dramatically change the fractionation of Eu^{2+} and Eu^{3+}. Partition experiments for Eu, Sm, and Gd for both low-Ca and high-Ca pyroxene by Musselwhite et al. (2003, 2004), McKay (1989), and McKay et al. (1986) indicate that with increasing Ca in pyroxene, the Eu anomaly (Eu/Eu*) either should remain the same or decrease. For example, at IW D_{Eu}/D_{Gd} is ~0.3 for pigeonite (Musselwhite et al. 2003, 2004; McKay et al. 1986), ~0.55 for aluminous ("fassaitic") high-Ca pyroxene (McKay 1989), and ~0.4 for high-Ca pyroxene (Musselwhite et al. 2003, 2004). This relative behavior for Eu^{2+} and Eu^{3+} is also predicted from pyroxene Onuma diagrams and lattice strain models for pyroxene (i.e., Yurimoto and Sueno 1987; Blundy and Wood 1994, 2003; Lundstrom et al. 1998).

Lunar basalts 15058 and 15499 illustrate the relationship between Eu/Eu* and increasing Ca in the M2 site without the interference of plagioclase crystallization. In both cases, with increasing Ca, the Eu anomaly in the pyroxene becomes increasingly negative. In addition, when plagioclase becomes a liquidus phase in 15058, Eu/Eu* in the high-Ca pyroxene increases. This observation indicates that factors other than the increase of Ca in the M2 site are involved in the behavior of Eu^{2+} and Eu^{3+} in pyroxene.

Although Ca in the M2 site will affect the Eu anomaly in pyroxene at fairly reducing conditions, the variations in Eu/Eu* in 15058 and 15499 between A and B in Figure 6 may be related more closely to changes in melt composition and minor-element substitution into pyroxene. Along A → B, the increase of Al/Si in the pyroxene (Fig. 5) reflects an increase in Al (and the plagioclase component) in the melt. The degree of enrichment in Al and plagioclase component in the melt is more extreme in basalt 15499 than 15058 due to the delay of plagioclase crystallization. This appears to be correlated to the further decrease in Eu/Eu* in 15499 (Fig. 6). Once plagioclase begins to crystallize from the melt in 15058, the Al content of the melt decreases and the Eu/Eu* appears to increase. This behavior suggests that as Al in the melt increases, Sm, Eu^{3+}, and Gd will be partitioned increasingly into the M2 site and that Eu^{2+} will become retained increasingly in the melt. This is the product of two potential processes. First, as the Al content in the melt increases, so does the Al content in the coexisting pyroxene. Increased substitution of Al for Si into

the pyroxene tetrahedral (T) site should increase the capability for the pyroxene structure to charge balance the substitution of additional trivalent REE into the M2 site. For example: $^{T}Si^{4+} + {}^{M2}R^{2+} \rightarrow {}^{T}Al^{3+} + {}^{M2}REE^{3+}$. This substitution will enhance the *D*-values for the REE^{3+} while having no or the opposite effect on the *D*-value for divalent Eu (and Sr^{2+}). Previously McKay et al. (1994a, b), Lundstrom et al. (1998), and Schwandt and McKay (1998) have documented the effect of Al on the substitution of trivalent REE into pyroxene. Furthermore, Lundstrom et al. (1998) and Schwandt and McKay (1998) demonstrated that with increasing Al and $D^{REE^{3+}}$ for pyroxene, the D^{Eu} ($Eu^{3+} + Eu^{2+}$) and D^{Sr} does not increase as much or actually decreases. Alternatively, or in addition, the increase in the activities of network-forming plagioclase components in the melt during pyroxene crystallization may have a profound effect on the behavior of trivalent REE and limited effect on divalent Eu. In the examination of trace-element partitioning between titanite and silicate melt, Prowatke and Klemme (2005) showed that the partitioning behavior of trivalent cations was affected much more by melt structure than that of divalent cations. Lundstrom et al. (1988) and Schwandt and McKay (1998) demonstrated that Al in the melt has a significant effect on trivalent REE partitioning, but only a minimal or opposite effect on Sr^{2+} and by analogy Eu^{2+}. Neither study was able to deduce if the dominant influence on trivalent REE and Eu^{2+} was the Al content of the melt or pyroxene.

Cooling and crystallization history

The selection of the basalts for this study was based on their different cooling rates and differences in crystallization relationships between pyroxene and plagioclase. It appears that both factors have an integral and profound effect on Eu/Eu* in pyroxene. As shown above, the cooling rate has an acute kinetic effect on the composition of the evolving melt and the suppression of the nucleation of plagioclase (Grove and Bence 1977). The differences in the timing of plagioclase appearance in the crystallization sequence and the kinetics of plagioclase nucleation clearly affect Eu/Eu* in pyroxene. The appearance of plagioclase both changes the Al content of the pyroxene and melt, which we have shown to influence Eu/Eu* and provides a crystallographic site that competes with pyroxene for Eu. The Al content of the melt and pyroxene and the availability of the X-site in plagioclase have opposite consequences on Eu/Eu*.

In lunar basalt 75035, plagioclase precedes the crystallization of pyroxene and continues to co-crystallize with pyroxene. The co-crystallization of these two phases results in a continual decrease in both Al and Eu in the melt and a corresponding decrease in Al/Si and Eu/Eu* in the pyroxene with Fe enrichment. In Pasamonte, it appears that the earliest pyroxene cores preceded plagioclase crystallization. This appears to be consistent with the experimental studies of Stolper (1977). This is reflected in the substantial variation in Al/Si and Eu/Eu* in the early pyroxene that reflects the changes in the crystallizing assemblage from pigeonite to pigeonite + plagioclase. Following this initial decrease in Eu/Eu*, the Eu anomaly remains constant. In pigeonite basalt 15058, plagioclase crystallization initially is suppressed. This caused the melt coexisting with the pyroxene to become oversaturated with plagioclase. Once plagioclase crystallized, there was a dramatic decrease in Al in the melt resulting in an initial increase in Eu/Eu* that was followed by a decrease in this ratio as plagioclase continued to crystallize. In pigeonite basalt 15499, plagioclase either never became a liquidus phase or appeared only after 98% of pyroxene crystallized. Therefore, plagioclase had little effect on Eu/Eu* in the pyroxene. The deepening of the negative Eu anomaly is a product of the melt composition being highly oversaturated with a plagioclase component.

How does the melt respond to the depletion of Eu^{2+} resulting from plagioclase co-crystallization with pyroxene? Are these systems buffered such that Eu^{2+}/Eu^{3+} in the melt remains constant or is this ratio not buffered in the melt at all? Shearer et al. (1989) concluded from a smaller data set of pyroxene analyses that in basalts that crystallized at f_{O_2} conditions of IW-1, the Eu^{2+}/Eu^{3+} in the melt was buffered. This appears to be consistent with the consensus opinion that most lunar basalts crystallize along an f_{O_2} path that parallels the IW buffer. The variation in Eu/Eu* in Figure 6 appears to present a much more complex picture. In Pasamonte, the pyroxene that co-crystallizes with plagioclase exhibits a limited variation in Eu/Eu*. On the other hand, the pyroxene in 75035 exhibits a constant decrease in Eu/Eu* along the Fe-enrichment trend of the pyroxene. Pyroxene in 15058 exhibits a more subtle decrease in Eu/Eu* with Fe-enrichment. However, we contend that this does not represent deviation from a buffered to an unbuffered Eu^{2+}/Eu^{3+}, but simply represents the depletion of Eu^{2+} by plagioclase and the depletion in the melt of Eu^{3+} (relative to the other trivalent REE) due to the buffered nature of the system. Much more compelling evidence must be revealed to make the argument that these systems do not buffer the Eu^{2+}/Eu^{3+}. Table 1 summarizes the relationship among the factors/processes and parameters.

Growth surfaces

Many of the pyroxenes in lunar pigeonite basalts exhibit well-defined growth surfaces or growth sectors (Bence and Papike 1971, 1972). In these basalts, Bence and Papike (1972) observed

TABLE 1. Effects of factors/processes on parameters

	Trace element and melt parameters					
Factors and processess	D(Sm)	D(Eu^{2+})	C(Eu)/C(Sm) in melt	Al in melt	Eu/Eu* in PYX	Melt Poly.
Increasing Wo	↑	↑†	↔	—	↔	—
Decreasing Wo	↓	↓†	↔	—	↔	—
Increasing Melt Poly.	↑	↔	↔	—	↓	—
Decreasing Melt Poly.	↓	↔	↔	—	↑	—
Pyroxene crystallization	↑‡	↔	↓	↑	↓	↑
Plagioclase crystallization	↓§	↔	↓	↓	↓‖	↓

† Data presented here and in other studies do not clearly document this effect.
‡ Consequence of increase in melt polymerization (Poly.) resulting from pyroxene crystallization.
§ Consequence of decrease in melt polymerization resulting from plagioclase crystallization.
‖ Depends on the relative importance of the increase in D(Sm) as result of less melt polymerization or depletion of Eu by plagioclase crystallization. The latter is probably more important in most situations.

that the growth sector normal to (110) was more enriched in Mg and Cr and depleted in Ti and Al relative to the growth sector normal to (010). Shearer et al. (1989) and Shearer and Larsen (1994) observed that, in general, the (010) sector was more enriched in incompatible elements (REE, Zr), depleted in compatible elements (V, Cr), and had a larger negative Eu anomaly. Schwandt and McKay (1998) made a similar observation. In their experimentally grown, sector-zoned pyroxenes, the (010) growth sector had higher Al and REE than the other sectors that they identified. Furthermore, they noted that the (010) and (100) sectors, in general, had larger negative Eu anomalies. Shearer and Larsen (1994) concluded that the behavior of trivalent REE and Eu in these different sectors was a function of growth rate and the geometry of tetrahedral, M1, and M2 sites on the growth surface. The (010) sector growth surface consists of alternating M2-tetrahedral and M1-tetrahedral layers. This configuration facilitates coupled substitutions by placing trivalent cations (Al, REE) into the M2 or M1 sites as well as the tetrahedral site.

Comparison between the behavior of Eu^{2+}-Eu^{3+} and V^{3+}-V^{4+} in pyroxene at IW-1

In addition to Eu, the valence state of V in glass and olivine has been utilized successfully as an oxybarometer for magmatic systems over a fairly broad range of f_{O_2} (Canil and Fedortchouk 2001; Sutton et al. 2005; Karner et al. 2003, 2006b; Shearer et al. 2005). Whereas Eu in basaltic melts consists of sub-equal portions of Eu^{2+} and Eu^{3+} at IW-1, the valence state of V at this f_{O_2} consists primarily of V^{3+} with a smaller proportion of V^{4+} (Fig. 1). The amount of V^{2+} is extremely minor if it is present at all (Sutton et al. 2005). A companion paper by Karner et al. (2006a) in this volume illustrates the behavior of V in pyroxene over a broad range of f_{O_2}, from IW-1 to QFM+0.5. Karner et al. (2006a) used the same basalts as are used in this study at f_{O_2} conditions of IW-1.

At IW-1, V predominantly substitutes into the octahedrally coordinated M1 site of pyroxene as V^{3+}. Karner et al. (2006a) suggested the following coupled substitutions for entry of V into pyroxene at reducing conditions: ${}^{T}Si^{4+} + {}^{M1}R^{2+} \rightarrow {}^{T}Al^{3+} + {}^{M1}V^{3+}$ and ${}^{M2}Ca^{2+} + {}^{M1}R^{2+} \rightarrow {}^{M2}Na^{1+} + {}^{M1}V^{3+}$. Furthermore, they concluded that the former coupled substitution would be the most important in volatile-poor (i.e., Na-, K-poor) magmatic systems such as the Moon and 4 Vesta.

At the outset, it would appear that the V-valence and Eu-valence pyroxene oxybarometers would be influenced by different variables, in addition to f_{O_2}, simply because these elements behave so differently. Trivalent V is compatible in pyroxenes and spinel, whereas it is incompatible in plagioclase. On the other hand, Eu is incompatible in pyroxene and spinel and at least divalent Eu is compatible in plagioclase. Vanadium occupies the M1 site in pyroxene, whereas the REE occupy the M2 site in pyroxene. Still, the common requirement of tetrahedral Al in coupled substitutions that accommodate trivalent REE into the M2 site and trivalent V into the M1 site results in the same variables influencing the behavior of both Eu^{2+} and Eu^{3+} and multiple valence states of V in pyroxene. For example, the delay in plagioclase crystallization in the two lunar pigeonite basalts influences the Al content of the melt and pyroxene, thereby increasing the D_V and $D_{Sm,Eu^{3+},Gd}$. This results in an increase in V and trivalent REE with increasing Ca content in the M2 site. Upon plagioclase crystallization, the V decreases in pyroxene because of the decrease in tetrahedral Al needed for charge balance in pyroxene. The REE increase in pyroxene as they remain incompatible and increase in the residual melt during crystallization. The similar effect of Al in pyroxene tetrahedral sites influences the usefulness of both V and Eu valence oxybarometers.

Effect of variables on the usefulness of the Eu valence oxybarometer

The Eu valence oxybarometer is a very powerful tool for estimating f_{O_2} during the crystallization of both terrestrial and extraterrestrial basalts. However, there are numerous variables that can influence the Eu/Eu* recorded in pyroxene that may compromise the determination of f_{O_2}. Experimental studies clearly show that Ca in the pyroxene M2 site will influence not only the capability of the M2 site to accommodate REE but will also result in small degrees of Eu^{2+}-Eu^{3+} fractionation. In addition to the influence of this major pyroxene component, Al content in the pyroxene and its influence on coupled substitutions will also influence the fractionation of Eu^{2+} from Eu^{3+}. For example, the coupled substitution ${}^{T}Si^{4+} + {}^{M2}R^{2+} \rightarrow {}^{T}Al^{3+} + {}^{M2}REE^{3+}$ may accommodate REE^{3+} into pyroxenes at the expense of Eu^{2+}. The growth rate and site configuration of pyroxene growth surfaces will have an effect on both incompatible-element partitioning and the fractionation of Eu^{2+} from Eu^{3+} into the pyroxene structure. Further influencing the fractionation of Eu^{2+} from Eu^{3+} is the Al content of the basalt, which will increase the activities of the network-forming components such as $CaAl_2O_4$ and $FeAl_2O_4$ in the melt during pyroxene crystallization. The melt composition, the appearance of plagioclase on the liquidus, and the kinetics of plagioclase crystallization may be influenced by the cooling rate. Finally, the data from these four basalts also suggest that Eu^{2+}/Eu^{3+} in the melt may remain buffered. The varied kinetics of plagioclase crystallization observed in these basalts does not seem to drive Eu^{2+}/Eu^{3+} significantly away from the buffering reaction. However, further investigation is needed.

If the f_{O_2} values determined from Eu behavior in pyroxene is not placed within a petrologic and crystal-chemical context, errors of 1 to 2 log units may result. Finally, the influence of these variables on the calculation of f_{O_2} may be reduced by using multiple, co-crystallizing phases (i.e., plagioclase and pyroxene) and ratioing Eu to adjacent REE (Sm,Gd). This was done by McKay et al. (1994b) to determine the oxidation conditions under which angrite LEW 86010 crystallized.

Acknowledgments

We thank both Dave Vaniman and Gordon McKay for their insightful comments on this manuscript. McKay's past work on deciphering trace-element behavior in pyroxenes has always proved to be motivating. This research was funded by the Cosmochemistry (J.J.P.) and Mars Fundamental Research (C.K.S.) programs of NASA. We appreciate their support.

References cited

Bence, A.E. and Papike, J.J. (1971) A martini glass clinopyroxene from the Moon. Earth Planetary Science Letters, 10, 245–251.

——— (1972) Pyroxene as recorders of lunar basalt petrogenesis: Chemical trends due to crystal-liquid interaction. Proceedings of the 3rd Lunar Science Conference, 1, 431–469.

Bence, A.E., Papike, J.J., and Prewitt, C.T. (1970) Apollo 12 clinopyroxenes: Chemical trends. Earth and Planetary Science Letters, 8, 393–399.

Bence, A.E., Papike, J.J., and Lindsley, D.H. (1971) Crystallization histories of clinopyroxenes in two porphyritic rocks from Oceanus Procellarum. Proceedings of the 2nd Lunar Science Conference, 1, 559–574.
Blundy, J. and Wood, B. (1994) Prediction of crystal-melt partitioning coefficients elastic moduli. Nature, 372, 452–454.
——— (2003) Partitioning of trace elements between crystals and melts. Earth and Planetary Science Letters (Frontiers), 210, 387–397.
Boyd, F.R., Jr. and Smith, D. (1971) Compositional zoning in pyroxenes from lunar rock 1201, Oceanus Procellarum. Journal of Petrology, 12, 439–464.
Brett, R., Butler, P.J., Meyer, C., Jr., Reid, A.M., Takeda, H., and Williams, R. (1971) Apollo 12 igneous rocks 12004, 12008, 12009, and 12022: A mineralogical and petrological study. Proceedings of the 2nd Lunar Science Conference, Geochimica et Cosmochimica Acta, Suppl. 2, 1, 301–317.
BVSP (Basaltic Volcanism Study Project) (1981) Basaltic volcanism on the terrestrial planets, 1286 p. Pergamon Press, New York.
Cameron, M. and Papike, J.J. (1981) Structural and chemical variations in pyrorene. American Mineralogist, 66, 1–50.
Canil, D. and Fedortchouk, Y. (2001) Olivine-liquid partitioning of vanadium and other trace elements, with applications to modern and ancient picrites. Canadian Mineralogist, 39, 319–330.
Delano, J.W. (1990) Experimental constraints on the oxidation state of the lunar mantle. Lunar and Planetary Science, XXI, 278–279.
Drake, M.J. (1975) The oxidation state of europium as an indicator of oxygen fugacity. Geochimica et Cosmochimica Acta, 39, 55–64.
Fogel, R.A. and Rutherford, M.J. (1995) Magmatic volatiles in primitive lunar glasses: I. FTIR and EPMA analyses of Apollo 15 green and yellow glasses and revision of the volatile-assisted fire-fountain theory. Geochimica et Cosmochimica Acta, 59, 201.
Grove, T.L. and Bence, A.E. (1977) Experimental studies of pyroxene-liquid interaction in quartz normative basalt 15597. Proceedings of the 8th Lunar and Planetary Science Conference, 1549–1579. Pergamon Press, New York.
Hanson, B. and Jones, J.H. (1998) The systematics of Cr^{3+} and Cr^{2+} partitioning between olivine and liquid in the presence of spinel. American Mineralogist, 83, 669–684.
Jones, J.H. (2004) Redox conditions among the terrestrial planets. Lunar and Planetary Science, XXXV, abstract 1264. CD-ROM.
Karner, J.M., Papike, J.J., and C.K. Shearer (2003) Olivine from Planetary basalts: Chemical signatures that indicate planetary parentage and those that record igneous setting and process. American Mineralogist, 88, 806–816.
Karner, J.M., Papike, J.J., and Shearer, C.K. (2006a) Comparative planetary mineralogy: Major and minor element chemistry and the partitioning of vanadium into pyroxene from planetary basalts. American Mineralogist, 91, 1574–1582.
Karner, J.M., Sutton, S.R., Papike, J.J., Shearer, C.K., Jones, J.H., and Newville, M. (2006b) Application of a new Vanadium Valence Oxybarometer to Basaltic Glasses from Earth, Moon, and Mars. American Mineralogist, 91, 270–277.
Lofgren, G.E., Donaldson, C.H., and Usselman, T.M. (1975) Geology, petrology, and crystallization of the Apollo 15 quartz normative basalts. Proceedings of the 6th Lunar Science Conference, 79–99. Pergamon Press, New York.
Lundstrom, C.C., Shaw, H.F., Ryerson, F.J., Williams, Q., and Gill, J. (1998) Crystal chemical control of clinopyroxene-melt partitioning in the Di-Ab-An system: Implications for the elemental fractionations in the depleted mantle. Geochimica et Cosmochimica Acta, 62, 2849–2862.
McCanta, M.C. and Rutherford, M.J. (2002) Oxygen fugacity recorded in pigeonite: Indications of a heterogeneous martian magma source region? In A.H. Treiman and C.D.K. Herd, Eds., Unmixing the SNCs: Chemical, Isotopic, and Petrologic Components of Martian Meteorites, p. 35. LPI Contribution 1134, Lunar and Planetary Institute, Houston.
McKay, G.A. (1989) Partitioning of rare earth elements between major silicate minerals and basaltic melts. In B.R. Lipin and G.A McKay, Eds., Geochemistry and Mineralogy of Rare Earth Elements, 21, p. 45–77. Reviews in Mineralogy, Mineralogical Society of America, Chantilly, Virginia.
McKay, G., Wagstaff, J., and Yang, S.-R. (1986) Clinopyroxene REE distribution coefficients for shergottites: The REE content of the Shergotty melt. Geochimica et Cosmochimica Acta, 50, 927–937.
McKay, G.A., Le, L., and Wagstaff, J. (1994a) Synthetic and natural Nakhla pyroxenes: Parent melt composition and REE partition coefficients. Proceedings of the 25th Lunar and Planetary Science Conference, 883–884.
McKay, G.A., Le, L., Wagstaff, J., and Crozaz, G. (1994b) Experimental partitioning of rare earth elements and strontium: Constraints on petrogenesis and redox conditions during crystallization of Antarctic angrite Lewis Cliff 86010. Geochimica et Cosmochimica Acta, 58, 2911–2919.
McKay, G.A., Le, L., Schwandt, C., Mikouchi, T., Koizumi, E., and Jones, J. (2004) Yamato 980459: The most primitive shergottite? Lunar and Planetary Science Conference, XXXV, abstract 2154 (CD-ROM).
Musselwhite, D.S. and Jones, J.H. (2003) Oxygen fugacity of the martian mantle from pyroxene/melt partitioning of REE. Lunar and Planetary Science Conference, XXXIV, abstract 2032 (CD-ROM).
Musselwhite, D.S., Jones, J.H., and Shearer, C.K. (2004) Oxygen fugacity of the martian mantle from pigeonite/melt partitioning of Sm, Eu, and G. Workshop on Oxygen in the Terrestrial Planets, abstract 3027 (CD-ROM).
Papike, J.J. and Bence, A.E. (1978) Lunar mare vs. terrestrial mid-ocean ridge basalts: planetary constraints on basaltic volcanism. Geophysical Research Letters, 5, 803–806.
Papike, J.J., Hodges, F.N., Bence, A.E., Cameron, M., and Rhodes, J.M. (1976) Mare basalts: Crystal chemistry, mineralogy, and petrology. Reviews in Geophysics and Space Physics, 14, 475–540.
Papike, J.J., Ryder, G., and Shearer, C.K. (1998) Lunar Samples. In J.J. Papike, Ed., Planetary Materials, 36, p. 5-1–5-234. Reviews in Mineralogy, Mineralogical Society of America, Chantilly, Virginia.
Papike, J.J., Karner, J.M., and Shearer, C.K. (2005) Comparative planetary mineralogy: Valence state partitioning of Cr, Fe, Ti, and V among crystallographic sites in olivine, pyroxene, and spinel from planetary basalts. American Mineralogist, 90, 277–290.
Philpotts, J.A. (1970) Redox estimates from a calculation of Eu^{2+} and Eu^{3+} concentrations in natural phases. Earth and Planetary Science Letters, 9, 257–268.
Prowatke, S. and Klemme, S. (2005) Effect of melt composition on the partitioning of trace elements between titanite and silicate melt. Geochimica et Cosmochimica Acta, 69, 695–709.
Pun, A. and Papike, J.J. (1995) Ion microprobe investigation of exsolved pyroxene in cumulate eucrites: Determination of selected trace-element partition coefficients. Geochimica et Cosmochimica Acta, 59, 2279–2289.
Sato, M. (1976) Oxygen fugacity and other thermochemical parameters of Apollo 17 high-Ti basalts and their implications on the reduction mechanism. Proceedings of the 7th Lunar Science Conference, 1323–1344.
Schnetzler, C.C. and Philpotts, J.A. (1970) Partition coefficients of the rare earth elements between igneous matrix material and rock-forming mineral phenocrysts-II. Geochimica et Cosmochimica Acta, 34, 333–340.
Schwandt, C.S. and McKay, G.A. (1998) Rare earth element partition coefficients from enstatite/melt synthesis experiments. Geochimica et Cosmochimica Acta, 62, 2845–2848.
Shearer, C.K. and Larsen, L.M. (1994) Sector-Zoned Aegirine from the Ilimaussag Alkaline Intrusion, South Greenland. Implications for trace-element behavior in pyroxene. American Mineralogist, 79, 340–352.
Shearer, C.K., Papike, J.J., Simon, S.B., and Shimizu, N. (1989) An ion microprobe study of the intra-crystalline behavior of REE and selected trace elements in pyroxene from mare basalts with different cooling and crystallization histories. Geochimica et Cosmochimica Acta, 53, 1041–1054.
Shearer, C.K., Karner, J., Papike, J.J., and Sutton, S.R. (2004) Oxygen fugacity of mare Basalts and the lunar mantle. Application of a new microscale oxybarometer based on the valence state of vanadium. Lunar Planetary Science Conference, XXXV, abstract 1617.
Shearer, C.K., McKay, G.A., Papike, J.J., Karner, J., and Sutton, S.R. (2005) Valence State Partitioning of Vanadium Between Olivine-Melt in Olivine-Phyric Martian Basalts. Defining the f_{O2} of the Martian Mantle. AGU Fall Meeting, abstracts with programs.
Sobolev, A.V., Migdisov, A.A., and Portnyagin, M.V. (1996) Incompatible element partitioning between clinopyroxene and basalt liquid revealed by the study of melt inclusions in minerals from Troodos lavas. Cyprus.Petrology, 4(3), 307–317.
Stolper, E. (1977) Experimental petrology of eucrite meteorites. Geochimica et Cosmochimica Acta, 41, 587–611.
Sutton, S.R., Karner, J., Papike, J.J., Delaney, J.S., Shearer, C.K., Newville, M., Eng, P., Rivers, M., and Dyer, M.D. (2005) A new microscale oxybarometer for solar system basaltic glasses based on a vanadium K-edge XANES. Geochimica et Cosmochimica Acta, 69, 2333–2348.
Wadhwa, M. (2001) Redox state of Mars' upper mantle and crust from Eu anomalies in shergottite pyroxenes. Science, 291, 1527–1530.
Weill, D.F. and Drake, M.J. (1973) Europium anomaly in plagioclase feldspar: Experimental results and semiquantitative model. Science, 180, 1059–1060.
Weill, D.F. and McKay, G.A. (1975) The partitioning of Mg, Fe, Sr, Ce, Sm, Eu, and Yb in lunar igneous systems and a possible origin of KREEP by equilibrium partial melting. Proceedings of the 6th Lunar Science Conference, 1143–1158. Pergamon Press, New York.
Weill. D.F., McKay, G.A., Kridelbaugh, S.J., and Grutzeck, M. (1974) Modeling of the evolution of Sm and Eu abundances during lunar igneous differentiation. Proceedings of the 5th Lunar Science Conference, 1337–1352.
Yurimoto, H. and Sueno, S. (1987) Anion and cation partitioning between three pyroxenes, chrome spinel phenocrysts, and the host boninite magmas: an ion microprobe study. Geochemical Journal, 21, 85–104.

MANUSCRIPT RECEIVED SEPTEMBER 20, 2005
MANUSCRIPT ACCEPTED APRIL 11, 2006
MANUSCRIPT HANDLED BY DAVID VANIMAN